Dynamic Clustering in Suspension of Motile Bacteria

Xiao Chen[1], Xiang Yang[1], Mingcheng Yang[2] and H. P. Zhang[1,3] (a)

[1] *Department of Physics and astronomy and Institute of Natural Sciences, Shanghai Jiao Tong University, China*
[2] *Beijing National Laboratory for Condensed Matter Physics and Key Laboratory of Soft Matter Physics, Institute of Physics, Chinese Academy of Sciences, China*
[3] *Collaborative Innovation Center of Advanced Microstructures, Nanjing, China*

PACS 47.63.Gd – swimming of microorganisms
PACS 87.18.Gh – cell-cell communication
PACS 87.17.Jj – Cell locomotion,chemotaxis

Abstract –Bacteria suspension exhibits a wide range of collective phenomena arsing from interactions between individual cells. Here we show *Serratia marcescens* cells near an air-liquid interface spontaneously aggregate into dynamic clusters through surface-mediated hydrodynamic interactions. These long-lived clusters translate randomly and rotate in the counter-clockwise direction; they continuously evolve, merge with others and split into smaller ones. Measurements indicate that long-ranged hydrodynamic interactions have strong influences on cluster properties. Bacterial clusters change material and fluid transport near the interface and hence may have environmental and biological consequences.

Active systems are composed of self-propelled particles that can produce motion by taking in and dissipating energy [1–4]. Examples exist at different length scales, from bacteria suspension [5–10] to flocks of birds [11–13]. Being far from thermal equilibrium, active systems are not subject to thermodynamic constraints, such as detailed balance or fluctuation-dissipation theorem [14–16]. This renders the physics of active systems much richer than that of thermal systems. For example, collective motion with extended spatio-temporal coherence has been reported in many active systems [5–9, 11–13, 17–19]. Such coherent motion can arise from local interactions that align a particle's motion with its neighbors through biological coordination [11, 12] or physical interactions [17, 19].

Active systems without alignment interactions also exhibit interesting collective behavior. Theoretical models have shown that systems with a density-dependent motility phase separate into dense dynamic clusters and a dilute gas phase [14, 15, 20]. Numerical simulations of repulsive self-propelled disks confirmed the theoretical prediction of phase separation [21, 22]. Effects of motility, attractive interaction, and hydrodynamic forces have been extensively explored in simulations [23–26]. On the experimental side, dynamic clusters have been observed in Janus particles (platinum-coated [27] and Carbon-coated [28]) and colloidal particles with an embedded hematic cube [29]. Schwarz-Linek *et al* observed clusters of motile bacteria when they added polymers to bacteria suspension to induce depletion attraction between bacteria [30]. In a very recent paper [31], Petroff *et al* reported that *Thiovulum majus* bacteria form two-dimensional crystals near a liquid-solid interface. Understanding the origins and properties of these dynamic clusters may provide new insights into emergent behaviors of active matters and open up possibilities to build novel materials [15].

In this letter, we report experimental results for a new type of bacterial clusters formed near an air-liquid interface in a pure suspension without depletant agents. Fluid dynamic calculation and flow visualization are used to show surface-mediated hydrodynamic interactions can explain the formation of these clusters. We further quantify the statistical and dynamic properties of bacterial clusters and show long-ranged hydrodynamic forces have important influences on cluster properties. We conclude with discussions on related research and on possible technological and environmental implications of our work.

Experiments - Our experiments are carried out in drops of wild-type *Serratia marcescens* (ATCC 274) bacteria, which are propelled by a bundle of a few rotating flagella [32]. For cultivation, small amount of bacteria from frozen stock is put in 4 ml of Luria Broth (LB) growth

(a) E-mail:hepeng_zhang@sjtu.edu.cn

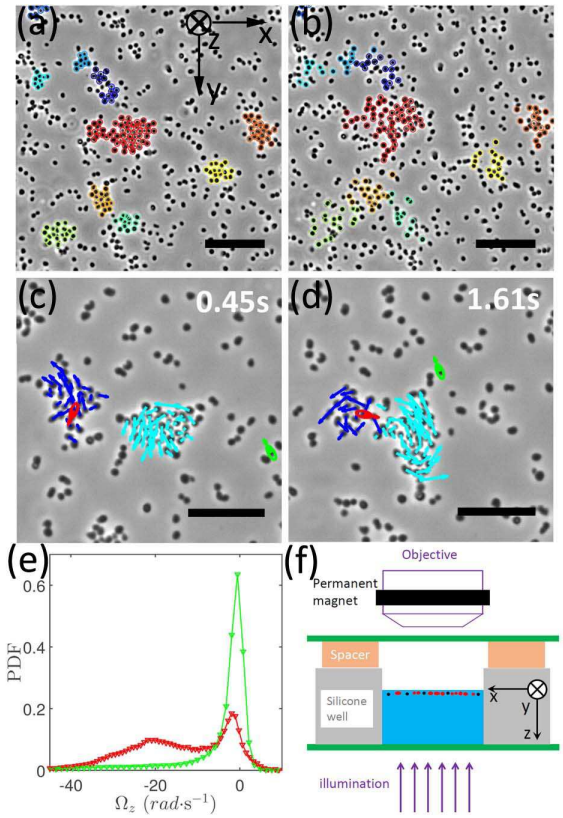

Fig. 1: (color online). (a) Dynamic clusters observed in a sample with bacterial density $\phi = 0.058\mu m^{-2}$. (b) Clusters dissolve after flagellar motor is damaged by strong light. The false colors in (a-b) show the time evolution of bacteria originally belonging to different clusters; image in (b) is taken 0.3 s after that in (a). (c-d) show a merging event of two clusters in a sample with $\phi = 0.044\mu m^{-2}$. Overlayed arrows show cell orientations. Two ellipses are drawn to highlight difference in cell motility in/outside clusters. (e) Probability density functions of averaged angular velocity of bacteria in(red) /outside(green) clusters. (f) Schematic of the experimental setup (not to scale). Scale bars in (a-b) and (c-d) correspond to 20 μm and 15 μm, respectively. A coordinate frame is defined in (a) and (f): the z axis points into the bulk fluid from the trapping (xy) plane.

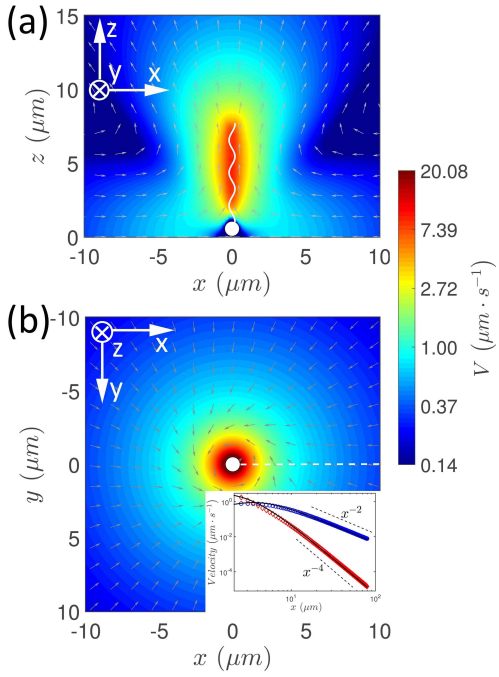

Fig. 2: (color online). Computed flow field around a model bacterium on two planes: y = 0 in (a) and z = 0.54 μm in (b). Color represents magnitude of velocity projection in the plane and arrows denote the direction of flow. Profiles of radial (blue) and tangential (red) velocity components along the white dashed line in (b) are plotted as symbols in the insert with fits (lines) to analytical expressions derived in Supplementary Text ST.pdf. Computation is carried out with the Regularized Stockslet method [35,36] and details can be found in Supplementary Text ST.pdf.

medium consisting of 0.5% yeast extract (Sangon G0961), 1% Tryptone (Sangon TN5250), and 1% NaCl (Sigma). Bacteria is incubated for 13 hours to a stationary phase in a shaking incubator which operates at 30°C and 200 rpm shaking speed. We then extract 1 ml bacteria solution and re-grow bacteria in 10 ml fresh LB growth medium supplemented with 5μg/ml of A22 for 4 hours at 33°C and 200 rpm. A22 is a small molecular inhibitor of a protein MreB, which is needed to maintain rod-like shape of many bacteria [33]. *S. marcescens* cells growing in a media with A22 are short ellipses with a mean aspect ratio of 1.2. The final bacteria solution is further diluted in distilled water to generate samples with various bacteria densities. To control bacterial motility, 1μg/ml photosensitizer FM 4-64 is added to the bacterial suspension [34]. In the presence of FM 4-64, the bacteria will be temporally paralyzed upon exposure to strong light. A 100W Mercury lamp(Nikon C-SHG1) is used to activate photodynamic effects.

Sample is enclosed in a sealed chamber (cf. Fig. 1(f)) which consists of a silicone well, a plastic spacer, and two cover slips (0.13 mm thick). The well has a diameter of 0.8 cm and a height of 0.1 cm. In some experiments, 1 μm super-paramagnetic tracer beads are added for flow visualization. Beads are confined to the interface by a permanent magnet and the strength of confinement can be tuned by moving the magnet relative to the sample. Two-dimensional bacterial or tracer motion in the trapping plane is imaged through a 60X phase contrast objective (Nikon ELWD ADL 60XC) and recorded by a camera (Basler acA2040-180km). We use a holographic microscope to measure three-dimensional motion of tracer particles and bacteria. A red LED is used for illumination and recorded holograms are analyzed by the Rayleigh-Sommerfeld back-propagation method to extract the spatial coordinates of the scatter [37,38].

Bacteria clusters - *S. marcescens* is known to adhere strongly to the air-liquid interface possibly due to hydrophobic interactions [39–41]. We use a holographic microscope to record such attaching events. Supplemen-

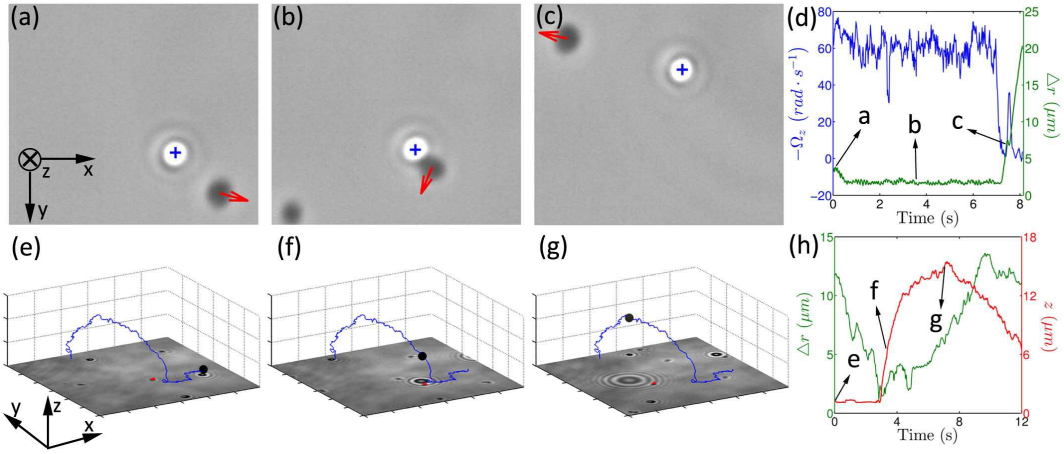

Fig. 3: (color online). (a-c) Interaction between a tracer bead (blue +) and a bacterium in the trapping plane. The red arrows mark the instantaneous orientation of cell body. (d) Time series of angular velocity (blue) of the cell and the separation (green) between the cell and bead. (e-f) Three-dimensional flow around a bacterium (red *) visualized by a tracer bead (black sphere). In each panel (e-g), the black-and-white image in xy plane is the raw hologram and the blue line is the tracer trajectory. (h) Time series of the z-coordinate of the tracer (red) and the separation (green) between the bead and the cell. Arrows in (d) and (h) mark when data in other panels are recorded.

tary movie S1.mp4 [1] shows two typical events: bacteria swim from the bulk towards the interface and get trapped near the interface. Trapped bacteria can move freely in the trapping (xy) plane; their centers-of-mass are tracked to quantify translational motion. Rotational motion is quantified by following the principal axes of the elliptical bacteria. The main control parameter in experiments is bacteria density in the trapping plane which is quantified by the number of bacteria per unit area and denoted as ϕ.

As shown in Fig. 1(a-b), trapped bacteria aggregate to form dynamic clusters which are identified through Voronoi analysis of bacterial positions (see Supplementary Text ST.pdf [2] for details). Clustering formation is a robust phenomenon and occurs under a wide range of bacteria densities and in various liquid environments including LB media, motility buffer, and water. However, formation of dynamic clusters requires bacterial motility. As shown in S2.mp4 [3], clusters dissolve immediately after we reduce the motility by using strong light [34]. Clusters reappear when bacteria motility is partially recovered after the light irradiation is stopped. Heavy metal ions ($CuSO_4$) are also used to reduce motility [42]; similar results are obtained.

To understand the connection between motility and cluster formation, we zoom-in and investigate how bacteria move in a cluster. We mark a bacterium in a cluster with a red ellipse in Fig. 1(c-d) (cf. S3.mp4 [4]); the marked bacterium rotates its body in the trapping plane with an angular velocity of $\Omega_z = -20$ rad/s. In contrast, a bacterium outside cluster (marked in green) shows little change in its body orientation. In Fig. 1(e) we plot the probability distribution functions of angular velocity, $P(\Omega_z)$, for bacteria in and outside clusters. While $P(\Omega_z)$ peaks around zero for bacteria outside clusters, $P(\Omega_z)$ shows a second peak at -23 rad/s for bacteria in clusters. We next use fluid dynamic calculation and flow visualization to show that the bacteria with large Ω_z can form clusters through hydrodynamic interactions.

Hydrodynamic interactions - *S. marcescens* bacteria swim by rotating their flagellar bundles. When viewed from the front (body) of a bacterium, the bundle rotates clockwisely and the cell body rotates in the opposite direction to achieve hydrodynamic torque balance. Fast body rotation in Fig. 1(e) suggests the bacteria in clusters orient their bundles perpendicular to the interface[5]. Bacteria in such a configuration can generate fluid flow that leads to cluster formation [31, 43, 44]. To illustrate the mechanism, we numerically compute fluid flow around a bacterial model that is oriented perpendicular to the interface. As shown in Fig. 2(a), the model has a 1-μm-diameter spherical body whose center is located at (0, 0, 0.54 μm) and is driven by a rotating flagellum. The translational degrees of freedom are frozen for the model. The model bacterium exerts a force in the positive z direction on the fluid, draws

[1] The movie S1.mp4 shows the bacterium trajectory as a blue line and the raw hologram as a black-and-white image. A black dot marks the instantaneous position of the bacterium. The objective is focused on the interface. All submitted movies are compressed in Xvid Codec and movies in MJPG format are available at:
`http://ins.sjtu.edu.cn/people/hpzhang/EPL/Movies.rar`

[2] ST.pdf contains detailed information of data analysis procedures and of fluid dynamic analysis and is available at:
`http://ins.sjtu.edu.cn/people/hpzhang/EPL/ST.pdf`.

[3] The movie S2.mp4 shows identified clusters in colors on phase-contrast images. Light irradiation starts at 16.8 s in the video.

[4] In the movie S3.mp4, phase-contrast images are shown in the background, cell orientations are marked by arrows, and ellipses are used to highlight two bacteria.

[5] A hydrodynamic mechanism was proposed to explain perpendicular orientation of *T. majus* cells [31]. Such a mechanism only works at a no-slip boundary and doesn't apply in the case of *S. marcescens* near a liquid-air interface.

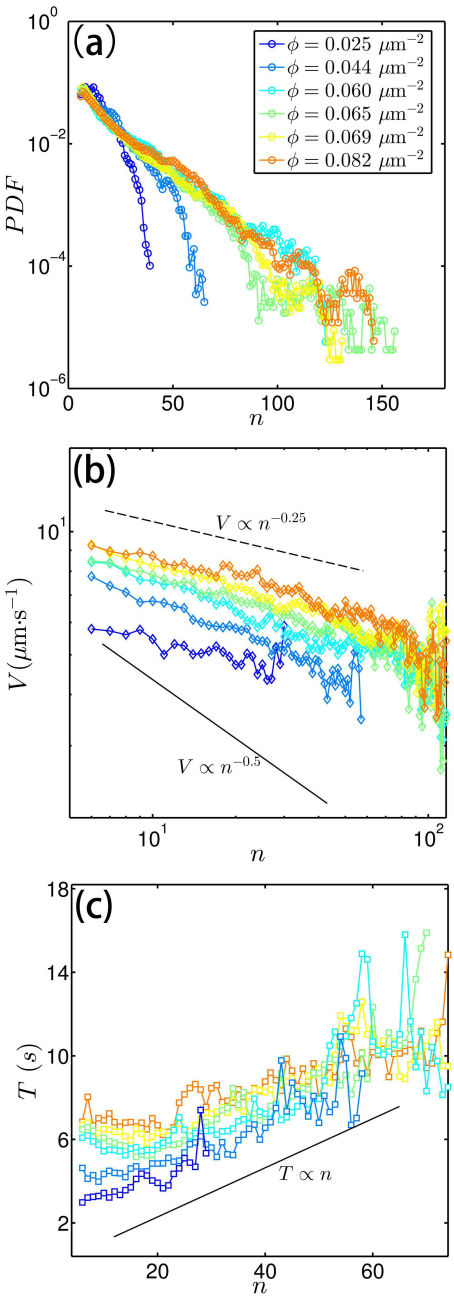

Fig. 4: (color online). Statistic and dynamic properties of clusters measured for six different bacterial densities (color-coded according to the legend in (a)). Quantities measured include probability distribution function (a), mean translation speed (b) and mean rotation period (c). Solid lines in (b) and (c) are salings derived from force and torque balance (see text).

in fluid along the interface (at $z = 0$) and pushes fluid to the bulk. Rotation of the flagellum and cell body also produces a tangential flow component that can be seen in Fig. 2(b), especially in the region close to the cell body. In the far field, radial ($V_r(r)$) and tangential ($V_\theta(r)$) components decays as: $V_r(r) \propto r^{-2}$ and $V_\theta(r) \propto r^{-4}$, as shown in the insert. Bacteria outside clusters in our experiments likely orient their bundle parallel to the interface and the cell body shows little rotation perpendicular to the interface, i.e. Ω_z is small [8, 9, 45].

Important flow features in Fig. 2 are qualitatively confirmed in experiments with two types of tracer beads. The first kind is strongly confined in the z-direction and only probes fluid flow in the trapping plane. A typical result is shown in Fig. 3(a-d) and Movie S4.mp4 [6]. A tracer bead is drawn to the bacterium from $t = 0$ to $t = 0.5$ s, which demonstrates the inward radial flow. While the bead and bacterium are bound, they rotate around each other counterclockwisely, which is a manifestation of the tangential flow in Fig. 2(b). At $t = 7$ s, the bacterium stops rotating and swims away from the bead. In the second experiment, a tracer bead is subject to weak confinement and can be advected also in the z-direction. As shown in Fig. 2(e-h) and Movie S5.mp4 [7], the bead is drawn towards the bacterium in the trapping plane until $t = 3.5$ s, when the separation between the bead and bacterium is about 1 μm. The bead is then advected quickly into the bulk, which demonstrates strong flow into the bulk around the bacterium.

Tracer particles are also used to visualize flow around bacteria clusters. Movie S6.mp4 [8] shows that clusters attract tracers and advect them into the bulk, mimicking results in Figs. 2 and 3. This supports the following picture: bacteria in clusters orient their flagella perpendicular to the interface; they generate inward radial flow that attracts neighbors to form clusters and counterclockwise tangential flow that drives clusters into rotation.

Cluster properties - Bacteria clusters observed in experiments are highly dynamic; they constantly evolve and change their sizes. We defined cluster size as the number of the constituent bacteria, n. Probability distribution functions for finding a cluster of a given size at six bacteria densities ϕ are shown in Fig. 4(a) . As the density increases, probability to find large clusters increases. Probability distribution function decays exponentially for large n. Similar exponential distributions have been observed in many previous studies [8,9] and may be modeled by fusion-fission processes [46].

We compute the following quantities to quantify translation and rotation of the Ith cluster which contains the ith bacterium at a location $\vec{r}_{i,I}$ and with a velocity $\vec{v}_{i,I}$. The center-of-mass of the Ith cluster is located at $\vec{R}_I = \langle \vec{r}_{i,I} \rangle_i$, where $\langle \cdot \rangle_i$ denotes an average over all n_I bacteria in the Ith cluster. Speed of the center-of-mass is $V_I = \left| \vec{V}_I \right| = \left| \langle \vec{v}_{i,I} \rangle_i \right|$. The angular speed of the Ith

[6] In the movie S4.mp4, a passive tracer confined to the interface visualizes attractive flow around a rotating bacterium.

[7] The Movie S5.mp4 shows three-dimensional motion of a passive tracer around a rotating bacterium.

[8] Movie 6 shows three-dimensional motion of a passive tracer around bacterial clusters. A 1μm tracer bead (marked by red+) is drawn towards a bacterial cluster during the first 1.7s, and then advected quickly into the bulk, as shown by the enlarging interference rings in the hologram.

cluster is defined as: $\omega_I = \left| \frac{\left\langle (\vec{r}_{i,I} - \vec{R}_I) \times (\vec{v}_{i,I} - \vec{V}_I) \right\rangle_i}{\left\langle (\vec{r}_{i,I} - \vec{R}_I) \cdot (\vec{r}_{i,I} - \vec{R}_I) \right\rangle_i} \right|$, whose inversion is the rotation period: $T_I = \frac{1}{\omega_I}$. Averaging V_I and T_I over all clusters of size n, we have mean translation speed $V(n) = \langle V_I \rangle_{n_I=n}$ and mean rotation period $T(n) = \langle T_I \rangle_{n_I=n}$.

Results in Fig. 4 (b-c) show that, for a given ϕ, larger clusters translate and rotate slower than smaller ones. This dependence is qualitatively consistent with a simple model of active clusters made of self-propelled particles [31]. Each particle is driven by a propulsive force F_{sp} in the $\hat{e}_i$ direction and has a drag coefficient of γ; they interact through pair-wise forces in the radial and tangential directions . If n particles in a cluster are randomly oriented, total propulsive force on the cluster is $|\sum_i F_{sp}\hat{e}_i| = F_{sp}n^{0.5}$. The total friction coefficient is the sum of all particles: $n\gamma$. The average velocity of the center-of-mass is the ratio of the total force to the total friction coefficient and scales as: $V \propto n^{-0.5}$. Using a similar torque-balance argument [31,47], we can get a scaling law for rotation period: $T \propto n$. These two scalings are shown in Fig. (b) and (c) as black lines; discrepancies with experimental results can be clearly seen.

First, we notice that cluster motion in experiments depends strongly on global densities, ϕ. Fig. 4 (b-c) show that a cluster of a given size translates faster and rotates slower in a system with a higher density. The dependence on system density likely arises from long-ranged hydrodynamic interactions which enable fluid disturbances to propagate far and couple different clusters over large distances. Second, Fig. 4(b) shows that cluster velocity $V(n)$ scales as $V \propto n^{-0.25}$ rather than $V \propto n^{-0.5}$. This is also possibly related to hydrodynamic interactions which determine how cluster friction and net propulsive force scale with cluster size. In the limit of Stokes drag, cluster friction scales as $\sqrt{n}$ [48] in two dimensions, which suggests that net propulsive force of clusters may scale as $n^{0.25}$. Data in Fig. 4(b-c) indicate that hydrodynamic interactions in our experiments are too complex to be represented by simplified pair-wise forces,.

Discussion - Inward radial flow in Fig. 2(a) is similar to feeding flow that many micro-organisms use to gather food from the fluid environment near an interface [43,44]. The same flow pattern is also used to explain the formation of bound *Volvox* pair [49] and to explain the attractive force between thermophoretic colloids [50–52]. Such an attractive boundary flow should exist near any low-Reynolds number swimmer that is oriented perpendicular to a fluid or solid boundary and swims into the boundary; consequently, these oriented swimmers experience effective attraction and can be hydrodynamically assembled into clusters. This provides a new mechanism, besides phoretic [29], depletion [30] interactions and self-trapping effects [28], to generate clusters of active particles.

Petroff *et al* [31] recently reported that *T. majus* bacteria form two-dimensional crystals near a liquid-solid interface through a mechanism similar to that in *S. marcescens* clusters. However, *T. majus* and *S. marcescens* systems are significantly different in at least two aspects. First, the strength of attractive interaction is different. Petroff *et al* used the product of propulsive force and swimmer size to estimate the energy scale (denoted as E) for attraction between cells. *T. majus* have an average diameter of 8.5 μm and swim at a speed of 600 $\mu m/s$; it was found that the attractive energy is much larger than thermal energy: $E \sim 10^4 k_B T$. Consequently, *T. majus* crystals are very stable and can contain up to a thousand cells. On the other hand, *S. marcescens*, like many other commonly studied bacteria [7, 18, 30] and artificial swimmers [28, 29], are approximately ten times smaller in both size and speed than *T. majus*; the attractive energy scale is 1000 times smaller and is on the order of $10k_BT$. Therefore, fluctuations play a more important role in the *S. marcescens* system and render *S. marcescens* clusters dynamic and constantly evolving. Second, *T. majus* crystals and *S. marcescens* clusters form near different hydrodynamic boundaries. A no-slip boundary makes the hydrodynamic attraction, f, between two *T. majus* cells decays rapidly as their separation, r, increases: $f \sim r^{-4}$; for *S. marcescens* clusters near a free-slip boundary, we have $f \sim r^{-2}$. Consequently, while hydrodynamic interaction between *T. majus* cells are severely screened, Fig. 4 shows that long-ranged hydrodynamic interactions influence *S. marcescens* clusters properties.

Conclusion - In summary, we have investigated dynamic clusters of *S. marcescens* bacteria near an air-liquid interface. Fluid dynamic calculation and flow visualization suggest that the constituent bacteria of these clusters orient their flagella perpendicular to the interface. Bacteria in such a configuration generate radial flow that attracts neighbors to form clusters and tangential flow that sets clusters into counter-clockwise rotation. We measured statistical properties of bacteria clusters and showed cluster properties are affected by long-ranged hydrodynamic interactions. *S. marcescens* clusters efficiently change material and fluid transport near the air-liquid interface; they may have environmental and biological consequences [6].

* * *

We acknowledge financial supports of the NSFC (No. 11422427, No. 11404379), the Program for Professor of Special Appointment at Shanghai Institutions of Higher Learning (No. SHDP201301), and the Innovation Program of Shanghai Municipal Education Commission (No. 14ZZ030).

REFERENCES1

[1] Ramaswamy S., *Annual Review of Condensed Matter Physics*, **1** (2010) 323.

[2] Vicsek T. and Zafeiris A., *Physics Reports-review Section of Physics Letters*, **517** (2012) 71.

[3] Marchetti M. C., Joanny J. F., Ramaswamy S., Liverpool T. B., Prost J., Rao M. and Simha R. A., *Rev. Mod. Phys.*, **85** (2013) 1143.

[4] Elgeti J., Winkler R. G. and Gompper G., *Reports on Progress in Physics*, **78** (2015) 056601 (50 pp.).

[5] Wu X. L. and Libchaber A., *Phys. Rev. Lett.*, **84** (2000) 3017.

[6] Dombrowski C., Cisneros L., Chatkaew S., Goldstein R. E. and Kessler J. O., *Phys. Rev. Lett.*, **93** (2004) 098103.

[7] Sokolov A., Aranson I. S., Kessler J. O. and Goldstein R. E., *Phys. Rev. Lett.*, **98** (2007) 158102.

[8] Zhang H. P., Be'er A., Florin E. L. and Swinney H. L., *Proc. Natl. Acad. Sci. U. S. A.*, **107** (2010) 13626.

[9] Chen X., Dong X., Be'er A., Swinney H. L. and Zhang H., *Phys. Rev. Lett.*, **108** (2012) 148101.

[10] Gachelin J., Mino G., Berthet H., Lindner A., Rousselet A. and Clement E., *Phys. Rev. Lett.*, **110** (2013) 268103.

[11] Ballerini M., Calbibbo N., Candeleir R., Cavagna A., Cisbani E., Giardina I., Lecomte V., Orlandi A., Parisi G., Procaccini A., Viale M. and Zdravkovic V., *Proc. Natl. Acad. Sci. U. S. A.*, **105** (2008) 1232.

[12] Nagy M., Akos Z., Biro D. and Vicsek T., *Nature*, **464** (2010) 890.

[13] Cavagna A. and Giardina I., *Annual Review of Condensed Matter Physics, Vol 5*, **5** (2014) 183.

[14] Tailleur J. and Cates M. E., *Phys. Rev. Lett.*, **100** (2008) 218103.

[15] Cates M. E., *Reports On Progress In Physics*, **75** (2012) 042601.

[16] Cates M. E. and Tailleur J., *Epl*, **101** (2013) 20010.

[17] Narayan V., Ramaswamy S. and Menon N., *Science (80-)*, **317** (2007) 105.

[18] Zhang H. P., Be'er A., Smith R. S., Florin E. L. and Swinney H. L., *EPL*, **87** (2009) 48011.

[19] Bricard A., Caussin J.-B., Desreumaux N., Dauchot O. and Bartolo D., *Nature*, **503** (2013) 95.

[20] Cates M. E. and Tailleur J., *Annual Review of Condensed Matter Physics*, **6** (2015) 219.

[21] Fily Y. and Marchetti M. C., *Phys. Rev. Lett.*, **108** (2012) 235702.

[22] Redner G. S., Hagan M. F. and Baskaran A., *Phys. Rev. Lett.*, **110** (2013) 055701.

[23] Mognetti B. M., Saric A., Angioletti-Uberti S., Cacciuto A., Valeriani C. and Frenkel D., *Phys. Rev. Lett.*, **111** (2013) 245702.

[24] Zoettl A. and Stark H., *Phys. Rev. Lett.*, **112** (2014) 118101.

[25] Furukawa A., Marenduzzo D. and Cates M. E., *Physical Review E*, **90** (2014) 022303.

[26] Matas-Navarro R., Golestanian R., Liverpool T. B. and Fielding S. M., *Physical Review E*, **90** (2014) 032304.

[27] Palacci J., Cottin-Bizonne C., Ybert C. and Bocquet L., *Phys. Rev. Lett.*, **105** (2010) 088304.

[28] Buttinoni I., Bialke J., Kummel F., Lowen H., Bechinger C. and Speck T., *Phys. Rev. Lett.*, **110** (2013) 238301.

[29] Palacci J., Sacanna S., Steinberg A. P., Pine D. J. and Chaikin P. M., *Science*, **339** (2013) 936.

[30] Schwarz-Linek J., Valeriani C., Cacciuto A., Cates M. E., Marenduzzo D., Morozov A. N. and Poon W. C. K., *Proc. Natl. Acad. Sci. U. S. A.*, **109** (2012) 4052.

[31] Petroff A. P., Wu X.-L. and Libchaber A., *Phys. Rev. Lett.*, **114** (2015) 158102.

[32] Hesse W. R. and Kim M. J., *Journal of Microscopy-oxford*, **233** (2009) 302.

[33] White C. L., Kitich A. and Gober J. W., *Mol. Microbiol.*, **76** (2010) 616.

[34] Lu S. T., Bi W. G., Liu F., Wu X. Y., Xing B. G. and Yeow E. K. L., *Phys. Rev. Lett.*, **111** (2013) 208101.

[35] Cortez R., Fauci L. and Medovikov A., *Phys. Fluids*, **17** (2005) 031504.

[36] Rodenborn B., Chen C. H., Swinney H. L., Liu B. and Zhang H. P., *Proc. Natl. Acad. Sci. U. S. A.*, **110** (2013) E338.

[37] Sheng J., Malkiel E. and Katz J., *Appl. Opt.*, **45** (2006) 3893.

[38] Lee S.-H. and Grier D. G., *Opt. Express*, **15** (2007) 1505.

[39] Syzdek L. D., *Appl. Environ. Microbiol.*, **49** (1985) 173.

[40] Hejazi A. and Falkiner F. R., *J. Med. Microbiol.*, **46** (1997) 903.

[41] Rabani A., Ariel G. and Be'er A., *Plos One*, **8** (2013) e83760.

[42] Behkam B. and Sitti M., *Appl. Phys. Lett.*, **90** (2007) 023902.

[43] Roper M., Dayel M. J., Pepper R. E. and Koehl M. A. R., *Phys. Rev. Lett.*, **110** (2013) 228104.

[44] Pepper R. E., Roper M., Ryu S., Matsumoto N., Nagai M. and Stone H. A., *Biophys. J.*, **105** (2013) 1796.

[45] Di Leonardo R., Dell'Arciprete D., Angelani L. and Iebba V., *Phys. Rev. Lett.*, **106** (2011) 038101.

[46] Gueron S. and Levin S. A., *Math. Biosci.*, **128** (1995) 243.

[47] Yan J., Bae S. C. and Granick S., *Soft Matter*, **11** (2015) 147.

[48] Cremer P. and Lowen H., *Physical Review E*, **89** (2014) 022307.

[49] Drescher K., Leptos K. C., Tuval I., Ishikawa T., Pedley T. J. and Goldstein R. E., *Phys. Rev. Lett.*, **102** (2009) 168101.

[50] Weinert F. M. and Braun D., *Phys. Rev. Lett.*, **101** (2008) 168301.

[51] Di Leonardo R., Ianni F. and Ruocco G., *Langmuir*, **25** (2009) 4247.

[52] Yang M. and Ripoll M., *Soft Matter*, **9** (2013) 4661.